

1 ELM2.1-XGBfire1.0: Improving wildfire prediction by integrating a machine- 2 learning fire model in a land surface model

3 Ye Liu ¹, Huilin Huang ¹, Sing-Chun (Sally) Wang ¹, Tao Zhang ², Donghui Xu ¹, and Yang Chen ³

4 ¹ Pacific Northwest National Laboratory, Richland, WA, USA.

5 ² Brookhaven National Laboratory, Upton, NY, USA

6 ³ University of California, Irvine, California, USA

7 Correspondence to: ye.liu@pnnl.gov and hulin.huang@pnnl.gov

8 Abstract

9 Wildfires have shown increasing trends in both frequency and severity across the Contiguous United States (CONUS).
10 However, process-based fire models have difficulties in accurately simulating the burned area over the CONUS due to a
11 simplification of the physical process and cannot capture the interplay among fire, ignition, climate, and human activities. The
12 deficiency of burned area simulation deteriorates the description of fire impact on energy balance, water budget, and carbon
13 fluxes in the Earth System Models (ESMs). Alternatively, machine learning (ML) based fire models, which capture statistical
14 relationships between the burned area and environmental factors, have shown promising burned area predictions and
15 corresponding fire impact simulation. We develop a hybrid framework (ELM2.1-XGBFire1.0) that integrates an eXtreme
16 Gradient Boosting (XGBoost) wildfire model with the Energy Exascale Earth System Model (E3SM) land model (ELM)
17 version 2.1. A Fortran-C-Python deep learning bridge is adapted to support online communication between ELM and the ML
18 fire model. Specifically, the burned area predicted by the ML-based wildfire model is directly passed to ELM to adjust the
19 carbon pool and vegetation dynamics after disturbance, which are then used as predictors in the ML-based fire model in the
20 next time step. Evaluated against the historical burned area from Global Fire Emissions Database 5 from 2001-2019, the
21 ELM2.1-XGBFire1.0 outperforms process-based fire models in terms of spatial distribution and seasonal variations. The
22 ELM2.1-XGBFire1.0 has proved to be a new tool for studying vegetation-fire interactions, and more importantly, enables
23 seamless exploration of climate-fire feedback, working as an active component in E3SM.

24 1 Introduction

25 Recent wildfire outbreaks worldwide have raised alarms due to wildfires burning longer and more intensely in many regions,
26 posing significant threats to human livelihoods and biodiversity. In the past two decades, satellite-derived data suggest that the
27 global total burned area has declined by over 20%, primarily attributed to human influences (Jones et al. 2022; Andela et al.
28 2017). The continental United States (CONUS) has emerged as a hotspot for wildfires, where both climate change and human
29 activities have fueled a 42% increase in the burned area (Jones et al. 2022). Such expansive burned areas release an average
30 of 162 million tons of CO₂ and 0.9 million tons of PM_{2.5} annually into the atmosphere, resulting in over \$200 billion health
31 costs due to exposure to wildfire smoke (Samborska et al. 2024; JEC 2023). Accurate prediction of wildfire risks has become
32 an urgent need.

33 Traditional fire models, predominantly process-based models, simulate the behavior of individual wildfires using
34 theoretical equations for ignitions and fire spread (Hantson et al. 2016). These models explicitly simulate the number and size
35 of individual fires by incorporating parameterizations and parameters derived from laboratory or field experiments and
36 typically estimate the burned area by scaling up to the grid-cell level (Lasslop et al. 2014; Pfeiffer et al. 2013; Yue et al. 2014;
37 Li et al. 2012; Thonicke et al. 2010; Huang et al. 2020, 2021; Arora and Boer 2005; Burton et al. 2019). While process-based
38 wildfire models are effective in simulating global burned area distribution (Hantson et al. 2020), they often fall short of
39 accurately predicting the extent and temporal changes of wildfires over the CONUS (Forkel et al. 2019; Teckentrup et al.
40 2019). The climate and vegetation controls on the CONUS burned area and their relative importance are incorrectly represented,
41 leading to failures in burned area predictions regarding both spatial distribution and temporal variations (Forkel et al. 2019).
42 Human ignition and suppression are assumed to be linearly or log-linearly related to population density and the gross domestic
43 product (GDP), respectively (Jones et al. 2023; Li et al. 2013). This assumption overlooks a more nuanced picture of human
44 activities, such as road density, cultural differences, agricultural activities, and forest management policy (Jones et al. 2022;
45 Villarreal et al. 2022; Hanan et al. 2021; Miller et al. 2009; Turco et al. 2023; Haas et al. 2022). Process-based fire models are
46 often integrated with biogeochemical process-enabled land models (hereafter referred to as BGC model) within Earth system
47 models (ESMs) to predict fire disturbances on carbon allocation, which is then used to update energy balance, water budget,
48 and carbon fluxes in the land model. Incorrect simulation of burned areas over the CONUS induces large uncertainties in the
49 assessment of fire impacts using ESMs.

50 Recent advances have explored the application of machine learning (ML) techniques in wildfire prediction (e.g., Buch et
51 al. 2023; Li et al. 2023; Wang et al. 2021; Zhu et al. 2022). ML models offer the advantage of capturing nonlinear dependencies
52 and complex interactions between driving factors and fire dynamics, without the need for explicit understanding of physical
53 processes (Rodrigues and de la Riva 2014). Zhu et al. (2022) presented a deep neural network (DNN) scheme that surrogated
54 the process-based wildfire model with the Energy Exascale Earth System Model (E3SM) interface, demonstrating over 90%
55 higher accuracy in simulating global burned area. Wang et al. (2021) combined the local predictors, large-scale meteorological
56 patterns, and the eXtreme Gradient Boosting (XGBoost) algorithm to build an ML wildfire model, which improves the

57 temporal correlations of burned areas in several regions over the CONUS by 14–44%. Buch et al. (2023) developed a novel
58 stochastic machine learning (SML) framework, SMLFire1.0, with a high spatial resolution of 12 km over the Western U.S.
59 (WUS).

60 The newly developed ML fire models often focus on wildfire properties such as burned area, fire count, and fire emissions
61 (Wang et al. 2021; Buch et al. 2023). Despite the improved fire predictions, fire impacts on the ecosystem, climate, and human
62 community cannot be evaluated without integrating the wildfire process into the Earth system. In addition, climate change
63 impacts on the burned area, either directly through fire weather conditions, or indirectly through ecosystem productivity,
64 vegetation type, fuel loads, and fuel moisture – cannot be fully understood without explicitly representing the complex
65 interplays between climate, ecosystems, and fire. For instance, a warmer and drier climate has been shown to cause an eightfold
66 rise in the high-severity burned area from 1985 to 2017 over the WUS (Parks and Abatzoglou 2020). The corresponding
67 changes in fire dynamics may shift the vegetation species distribution from those originally low in resistance to wildfire to
68 those in high resistance or even benefiting from regular fire occurrence (Rogers et al. 2015; Huang et al. 2024). The fire-
69 adapted vegetation species, in turn, facilitate the frequent occurrence of wildfires. In this consideration, a full coupling of fire,
70 ecosystem, and climate is required to better predict fire changes and the corresponding impacts in a future climate.

71 Leveraging the accuracy of ML-based wildfire models and the representation of ecosystem-climate interactions in ESMs,
72 in this study, we have developed a novel hybrid framework to integrate a pretrained ML wildfire model with the E3SM land
73 model (ELM) to study the full atmosphere-vegetation-wildfire feedbacks. This integration facilitates a dynamic feedback loop
74 where outputs from the ML model (i.e., predicted burned areas) inform the land surface processes in ELM, which in turn
75 update the inputs for the ML model for subsequent predictions. This approach leverages the detailed physical understanding
76 of surface biogeophysical and biogeochemical processes provided by ELM and the predictive power of ML-based wildfire
77 models to create a more accurate and robust framework for wildfire prediction and impact assessment. The remaining sections
78 are arranged as follows: Section 2 introduces the ELM and ML wildfire model training method, coupling strategy, and datasets
79 used in this study; Section 3 presents the simulated burned area compared with observations and several process-based fire
80 models; discussion and conclusion are in Section 4.

81 **2. Materials and methods**

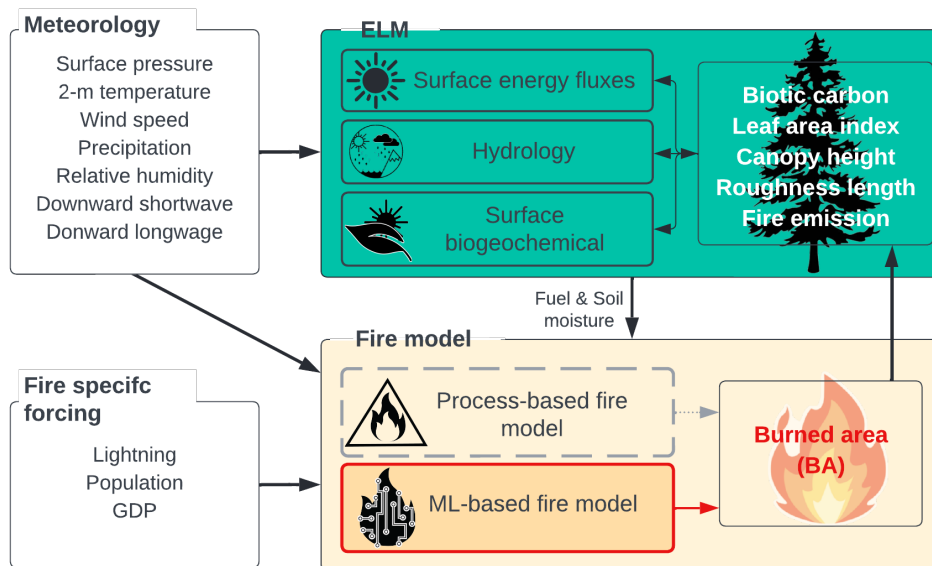
82 **2.1 Model Description**

83 **2.1.1 Default wildfire model in ELM**

84 The ELM is part of the E3SM project which started with a version of the Community Earth System Model (CESM1). The
85 ELM default wildfire module originated from the Community Land Model (CLM4.5) (Li et al, 2012). This wildfire model
86 calculates burned areas by multiplying the number of wildfires and burned area per fire on a grid-cell level. The number of
87 wildfires (fire count) is derived using anthropogenic and natural ignition sources, fuel load and combustibility, surface

88 meteorology, and anthropogenic suppression. The natural ignition source is derived from the number of cloud-to-ground
 89 lightning flashes multiplied by a constant ignition efficiency (Prentice and Mackerras 1977). Anthropogenic ignitions are
 90 simply parametrized using a fixed number of potential anthropogenic ignitions by a person and population density (Venevsky
 91 et al. 2002). Humans also suppress wildfires. The capability of fire suppression is assumed to be a function of GDP and
 92 population density. The ignition efficiency is also altered by fuel conditions, including the fuel load (aboveground biomass)
 93 and fuel combustibility (approximated using relative humidity, temperature, and top or root zone soil moisture). The spread of
 94 each fire is approximated using an ellipse shape with its length-to-breadth ratio determined by wind speed and fuel moisture
 95 (Rothermel 1972). This simple concept well captures the major constraints for predicting the global wildfire distribution and
 96 seasonal variations (Rabin et al. 2017; Li et al. 2014; Huang et al. 2020).

97 Like many other process-based wildfire models, the default fire model in ELM benefits from the full ecosystem interactions
 98 from its hosting land model, as well as the potential to be coupled with atmospheric models. With the BGC processes being
 99 turned on, ELM-BGC reallocates carbon and nitrogen in leaf, wood, root, litter, and soil pools after fire based on plant
 100 functional type (PFT)-dependent carbon combustion and mortality rate. The biogeochemical changes subsequently influence
 101 biogeophysical properties such as leaf area index (LAI), vegetation canopy height, and albedo, disturbing the land-atmosphere
 102 exchanges of energy and water fluxes. The post-fire vegetation recovery in ELM-BGC depends on the plant photosynthesis
 103 processes and PFT competition strategy for soil resources. The interactions between wildfire and vegetation under historical
 104 climate have been thoroughly assessed in CLM long-term simulations (Li and Lawrence 2017). The model framework is
 105 illustrated in Figure 1. Hereafter the ELM coupled with the process-based fire model is referred to as ELM-BGC.



106
 107 **Figure 1: Schematic diagram of the hybrid model framework.**

2.1.2 Machine learning wildfire model

The XGBoost-based wildfire model has proven to outperform process-based models in predicting burned areas over the CONUS (Wang et al. 2021). XGBoost is a highly efficient and scalable implementation of gradient boosting, designed for performance and speed (Chen and Guestrin 2016). It builds sequential decision trees to correct errors from previous models, using techniques like regularization to prevent overfitting and parallel processing for faster computation. In this study, we adapted the XGBoost algorithm used in Wang et al (2021) to develop an offline ML fire model using variables directly provided by ELM at each grid cell. Wang et al. (2021) integrated large-scale meteorological patterns alongside local weather, land surface properties, and socioeconomic data to enhance the prediction of burned areas. The large-scale patterns were identified using singular value decomposition (SVD) to capture influential atmospheric conditions that develop over days to weeks and cumulatively impact the monthly burned area. The feature importance analysis in their study noted that while large-scale patterns improved prediction, however, they played a secondary role. Therefore, we exclude the large-scale patterns from predictors without significantly affecting the model accuracy. Hereafter the uncoupled XGBoost fire model is referred to as offline-XGB.

2.1.3 Hybrid modeling framework

The offline-XGB model is integrated with the ELM using the ML4ESM coupling framework. The ML4ESM framework offers a robust and flexible solution for integrating ML parameterizations into ESMs through a Fortran-Python interface (Zhang et al. 2024). It supports popular ML libraries such as PyTorch, TensorFlow, and Scikit-learn, enabling the seamless incorporation of ML algorithms to represent complex climate processes like convection and wildfire dynamics. The interface leverages C language as an intermediary for efficient data transfer by accessing the same memory reference, instead of the extra data copy or through files, minimizing memory overhead and computational inefficiencies. A C-Hub is then used to communicate variables from the Fortran-written ELM and the Python-written ML fire model. In our application, all surface meteorology, lightning, and socioeconomic data, alongside the ELM simulated fuel conditions are passed to the ML-based fire model to predict the burned area. The burned area is returned to ELM to calculate fire impacts and update surface properties.

2.2 Datasets and processing

2.2.1 Burned area datasets

The primary dataset for training and validating the ML-based model is the Global Fire Emissions Database version 5 (GFED5) (Chen et al. 2023). The GFED5 is a succession of GFED4s (van der Werf et al. 2017), which we also use as an additional reference dataset. GFED4 is generated by fusing multiple streams of remote sensing data to create a 24-year (1997-2020) dataset of the monthly burned area at 0.25° spatial resolution. During 2001-2020, the GFED5 comprises the Moderate Resolution Imaging Spectroradiometer (MODIS) MCD64A1 burned area product (Hall et al. 2016; Giglio et al. 2016; Giglio et al. 2018), with adjustment for the errors of commission and omission. Adjustment factors are estimated based on region,

land cover, and tree cover fraction, using spatiotemporally aligned burned areas from Landsat or Sentinel-2 (Claverie et al. 2018). Because of a new fire detection method that significantly boosts the area of small fires, the CONUS annual burned increases from 2.36 Mha in GFED4s to 6.04 in GFED5, primarily contributed by the increase of crop fire from 0.83 Mha to 3.09 Mha.

The FireCCI5.1 is obtained as another reference dataset (Chuvieco et al. 2019). FireCCI5.1 maps fires at 250 m resolution using the spectral information from MODIS in combination with the thermal anomalies. FireCCI5.1 has been reported heavily underestimate the total burned area mainly due to under-representation of small fires (Lizundia-Loiola et al. 2020).

Besides observations, we also obtained burned area from seven state-of-the-art process-based wildfire models participating the Inter-Sectoral Impact Model Intercomparison Project (ISIMIP3a) (Burton et al. 2024), including the Canadian Land Surface Scheme Including Biogeochemical Cycles (CLASSIC) (Melton et al. 2020), the Simplified Simple Biosphere model coupled with the Top-down Representation of Interactive Foliage and Flora Including Dynamics model (SSiB4-TRIFFID-Fire) (Huang et al. 2020, 2021), the SPread and InTensity of FIRE (SPITFIRE) coupled with the Organizing Carbon and Hydrology In Dynamic Ecosystems (ORCHIDEE) (Yue et al. 2014), the Joint UK Land Environment Simulator (JULES) coupled with the INFERNO fire model (Mathison et al. 2023; Mangeon et al. 2016), the LPJ-GUESS dynamic global vegetation model coupled to the SPITFIRE (LPJ-GUESS-SPITFIRE) and SIMple FIRE model (SIMFIRE) (Smith et al. 2001) and BLAZE induced biosphere-atmosphere flux Estimator (BLAZE) (LPJ-GUESS-SIMFIRE-BLAZE) (Rabin et al. 2017), and the Vegetation Integrative Simulator for Trace gases (VISIT) (Ito 2019). Driven by GSWP3-W5E5 historical climate forcing (Cucchi et al. 2020; Lange et al. 2021), these models provides monthly burned area at 0.5° spatial resolution from 1901-2019. The multi-model output during 2001-2019 is used in this study. We also performed the benchmarking simulation using the built-in process model in ELM-BGC.

The process-based models differ from one another not only in their dynamic global vegetation models (DGVMs) but also in the complexity of their fire models. ELM-BGC and SSiB4-TRIFFID utilized the same fire model from Li et al. (2012), LPJ-GUESS-SPITFIRE and ORCHIDEE both coupled with SPITFIRE. Other models incorporate their own unique fire modules. The representation of fires over croplands and pastures varies across models (Burton et al. 2024; Teckentrup et al. 2019). Most models, except for JULES, classify croplands as non-burnable. JULES treats croplands similarly to natural grasslands, while all other models exclude croplands from burning. Most models do not include pasture as a PFT, therefore, do not distinguish pastures from grasslands in terms of both growth and fire behavior. In LPJ-GUESS-SIMFIRE-BLAZE, pastures are harvested, leading to reduced biomass and consequently a smaller burned area. The difference among process-based models will be discussed in Section 4.

2.2.2 Surface meteorological, lightning, and socioeconomic datasets

Surface meteorological variables, including temperature, humidity, wind speed, downward shortwave radiation, downward longwave radiation, precipitation, and surface pressure, are obtained from NLDAS-2 (Phase 2 of the North American Land

171 Data Assimilation System) forcing fields to both drive the ELM and construct the training set for the ML fire model. This
 172 dataset combines multiple sources of observations (such as precipitation gauge data, satellite data, and radar precipitation
 173 measurements) to produce estimates of climatological properties at or near the Earth’s surface at hourly temporal resolution
 174 and 1/8th-degree grid spacing. We use the temperature, relative humidity, specific humidity, wind speed, and precipitation
 175 directly from NLDAS-2 to train the ML fire model. Additionally, we calculate the Standardized Precipitation
 176 Evapotranspiration Index (SPEI) following (Beguería et al. 2014) and vapor pressure deficit (VPD) based on NLDAS-2 dataset
 177 as additional input for the ML model (Table 1). We coarsen this dataset to 0.25° to align with burned area datasets.

178 In addition to surface meteorological forcing, we acquire lightning and socioeconomic datasets from multiple sources,
 179 while identical to those used by ISIMIP3a fire models. The 2-hourly climatology lightning flashes data from NASA LIS/OTD
 180 v2.2 at 2.5° resolution are used to calculate the number of natural ignitions. The gridded population density data is acquired
 181 from Goldewijk et al. (2017), while the GDP per capita is from the World Bank (<https://data.worldbank.org/>). Lightning,
 182 population density, and GDP data are resampled to 0.25°×0.25° spatial using bilinear interpolation and annual temporal
 183 resolution using the nearest neighbor method. To train the ML model, additional inputs, including top-layer soil moisture, LAI,
 184 and spatial fraction of each plant functional type (PFT), are simulated by ELM (explained further in Section 2.3).

185 **Table 1 Meteorological forcing, land surface properties, and fire specific inputs for driving the ELM-BGC and training the offline-**
 186 **XGB fire model.**

Meteorological forcing		Land surface property	
Temperature	NLDAS-2	Soil moisture	ELM-BGC output
Relative humidity		Leaf area index	
Wind speed		Plant functional type (PFT) fraction	
Precipitation		Fire specific inputs	
Standardized precipitation evapotranspiration index (SPEI)		Lightning	NASA LIS/OTD v2.2
Vapor pressure deficit (VPD)		GDP	World Bank
		Population density	Goldewijk et al. (2017)

187 **2.3 Model configuration and offline-XGB training and coupling processes**

188 In ELM-BGC, vegetation properties, including canopy height and LAI, vary with carbon allocation and distribution, driven
 189 by climate variability and disturbances such as wildfires. To bring the model’s carbon and nitrogen pools into equilibrium, we
 190 first conduct long-term spin-up simulations as suggested by Lawrence et al. (2011). We adopt a two-step approach consisting
 191 of a 400-year accelerated decomposition (AD) spin-up followed by a 400-year regular spin-up, driven by cycling NLDAS-2
 192 meteorological forcing from 1981 through 2000. In the AD spin-up, acceleration factors will be applied to accelerate
 193 decomposition in soil organic matter pools, and for plant dead stem and coarse root mortality. The terrestrial carbon pools and
 194 vegetation distribution after spin-up simulations reach quasi-equilibrium states after the 800-year simulations.

195 Initialized with the quasi-equilibrium state from the spin-up simulation, we conduct transient simulations with the process-
196 based fire model in the ELM-BGC, driven by hourly NLDAS-2 meteorological forcings at a 0.25° resolution from 2001 to
197 2020. The process-based fire model operates on an hourly basis, matching the frequency of the meteorological inputs, while
198 the ML fire model is trained and applied at a monthly interval, consistent with GFED5 data intervals. For training the offline-
199 XGB model, the ELM-BGC outputs, including LAI, surface soil moisture, and PFT fractions, are averaged to monthly intervals,
200 combined with monthly mean meteorological conditions, socioeconomic variables (GDP, population density), and lightning
201 (as detailed in Table 1) to learn the relationship between predictors and burned area. To reduce overfitting, the 20-year dataset
202 is split, with 80% used for training and 20% for validation. During training, grid cells with fewer than 30 months of non-zero
203 burned area (~two-thirds of the total number of grid cells) are masked. This step is important to avoid feeding the ML model
204 distinct predictor combinations that all correspond to zero burned areas, which could skew the model's learning process. Model
205 performance was evaluated based on its accuracy in predicting the spatial distribution and temporal variation of burned areas.
206 Validation metrics included root mean square error (RMSE) and the coefficient of determination (R^2).

207 We then integrate the offline-XGB to ELM-BGC, forming the coupled model ELM2.1-XGBfire1.0. The coupled model
208 runs at 0.25° and hourly resolutions, where the hourly model predictions are accumulated to calculate monthly means. At the
209 end of each month, the ML fire model is called to predict the monthly burned area, updating the land surface properties (e.g.,
210 LAI and vegetation height), carbon cycling (biotic carbon in each pool), and ecohydrology processes (photosynthesis and soil
211 moisture) in ELM-BGC.

212 **2.4 Ecoregion**

213 We evaluate the model simulated burned area for each ecoregion adopted from the U.S. Environmental Protection Agency
214 (EPA). Ecoregions are areas where ecosystems (and the type, quality, and quantity of environmental resources) are generally
215 similar (Omernik and Griffith 2014) and generally, wildfire properties in each ecoregion are similar. A combination of level I
216 and level II ecoregions is used and some types have been combined to focus on the broad vegetation distribution. As shown in
217 Figure 2, the Western Forested Mountains include NW Forested Mountains, Marine West Coast Forests, and Mediterranean
218 California from ecoregion level 1. The North American (NA) Deserts include NA Deserts and small portions of Temperate
219 Sierras and Southern Semi-Arid Highlands. The Northeast (NE) Temperate Forests include Mixed Wood Shield, Mixed Wood
220 Plains, and Atlantic Highlands from ecoregion level II. The Southeast (SE) Temperate Forests include Southeastern U.S. Plains
221 Ozark, Ouachita-Appalachian Forests, and Mississippi Alluvial and Southeast U.S. Coastal Plains ecoregion level II.

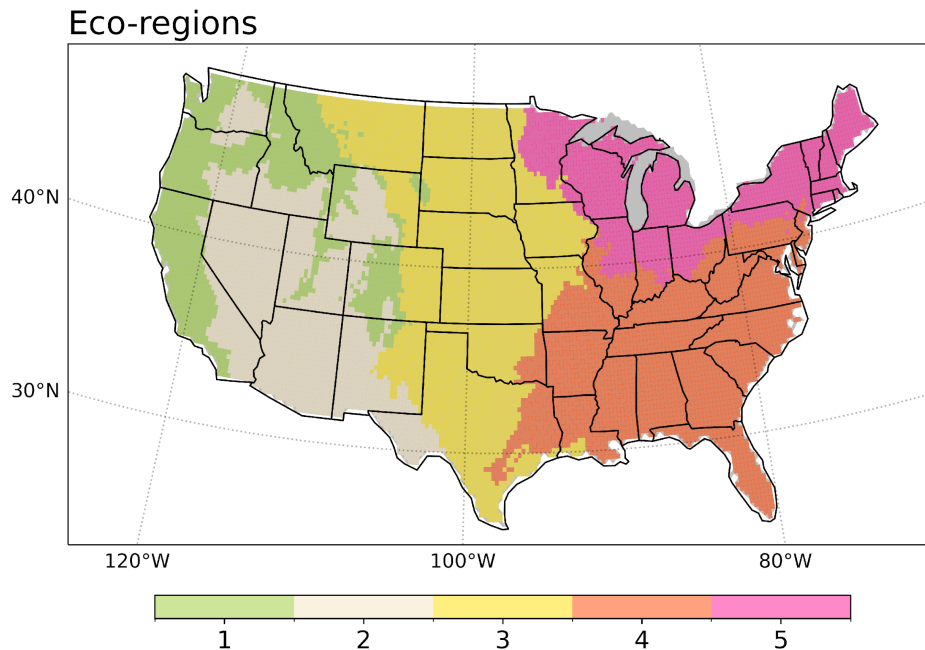


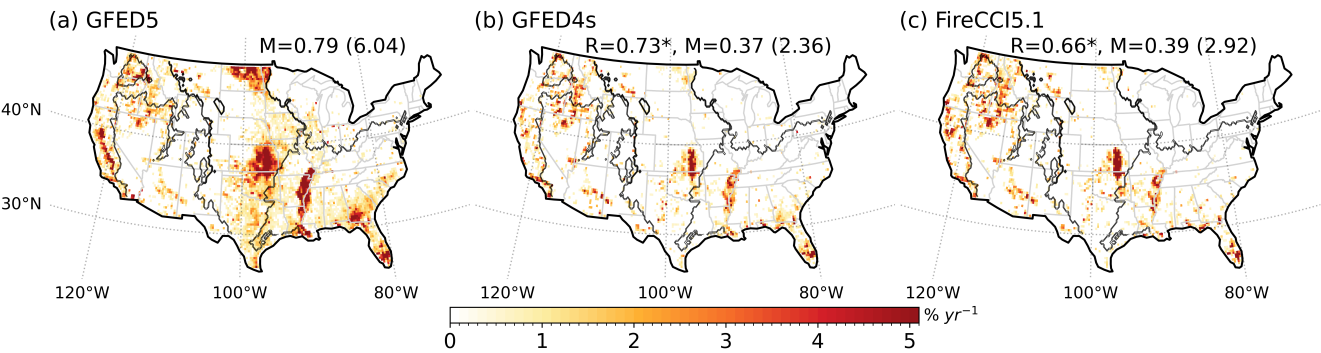
Figure 2: Ecoregions used in fire model evaluation. 1 – Western Forested Mountains, 2 – NA Desert, 3 – Great Plains, 4 – SE Temperate Forests, and 5 – NE Temperate Forests.

3 Results

3.1 Evaluation of the burned area spatial distribution

The burned areas across the CONUS exhibit a strong spatial variation (Fig. 3a), primarily influenced by climate, vegetation, and human activities. According to the GFED5, the CONUS experiences an average burned area fraction (BAF) of 0.6–0.9% yr^{-1} (4.8–7.1 Mha yr^{-1}). The BAF in the WUS (Western Forested Mountains and NA Desert) ranges between 0.4–0.9% yr^{-1} (1.1–2.3 Mha yr^{-1}). States like California, Oregon, and Nevada, as well as the Rocky Mountain region, including parts of Colorado and Wyoming, experience large wildfires. The wildfires in the Pacific Northwest and northern California are generally lightning-caused and occur in boreal forests (Balch et al. 2017), whereas those in southern California are primarily caused by human ignition in dry forests and shrublands. The Southwest, including Arizona and New Mexico, also sees significant burned areas in shrublands and dry forests. In the Great Plains, states such as Kansas and North Dakota also exhibit high burned areas, alongside with Texas and Oklahoma, with a BAF ranging between 0.7–1.3% yr^{-1} (1.6–2.9 Mha yr^{-1}). These high burned areas are primarily contributed by agricultural fires, particularly for cleaning crop residues and managing pastures (Donovan et al. 2020). The Southeastern U.S. experiences 0.9–1.5% yr^{-1} (1.5–2.6 Mha yr^{-1}) BAF annually, while the temperate forested areas covering Florida, Georgia, and the Carolinas, show lower burned areas compared to the West. The Midwest and Northeast exhibit sparse burned areas, with BAF mostly less than 0.16–0.25% yr^{-1} (0.2–0.3 Mha yr^{-1}). Burned areas in GFED4s

240 and FireCCI5.1 are much smaller than GFED5 due to the underrepresentation of small fires. The overall spatial distributions
 241 are generally consistent across the three datasets, as shown by the high spatial correlation coefficients (R_p).



242
 243 **Figure 3: Observed burned area fraction ($\% \text{ yr}^{-1}$). (a) GFED5 (2001-2019), (b) GFED4s (2001-2016), and (c) FireCCI5.1 (2001-2019).**
 244 **The numbers indicate the mean (M) burned area fraction and burned area (in Mha) in brackets for each dataset. The pattern**
 245 **correlation (R) against GFED5 is also shown, with an asterisk (*) denoting significance at the 0.01 level. Black contours outline the**
 246 **ecoregions.**

247 The offline-XGB wildfire model reproduces the burned area distribution over the CONUS well (Fig. 3b), with a R_p of 0.98
 248 ($p<0.01$) and a bias of -1.0 Mha yr^{-1} . While integrated with ELM, the performance degraded ($R_p=0.59$, $p<0.01$, bias= 1.9 Mha
 249 yr^{-1}) (Fig. 3d). This degradation is likely due to the fire-vegetation feedbacks. The aboveground biomass and fuel moisture
 250 from ELM-BGC have been used to train the offline-XGB prior to the coupled run within ELM. In the coupled simulation,
 251 ELM2.1-XGBfire1.0 updates the biotic carbon and fuel moisture based on the burned area simulated in the previous timestep.
 252 Consequently, differences in the simulated burned area compared to the process-based models are reflected in the biotic carbon
 253 and fuel moisture, accumulating over the 20-year simulation period and influencing the burned area simulation in subsequent
 254 timesteps.

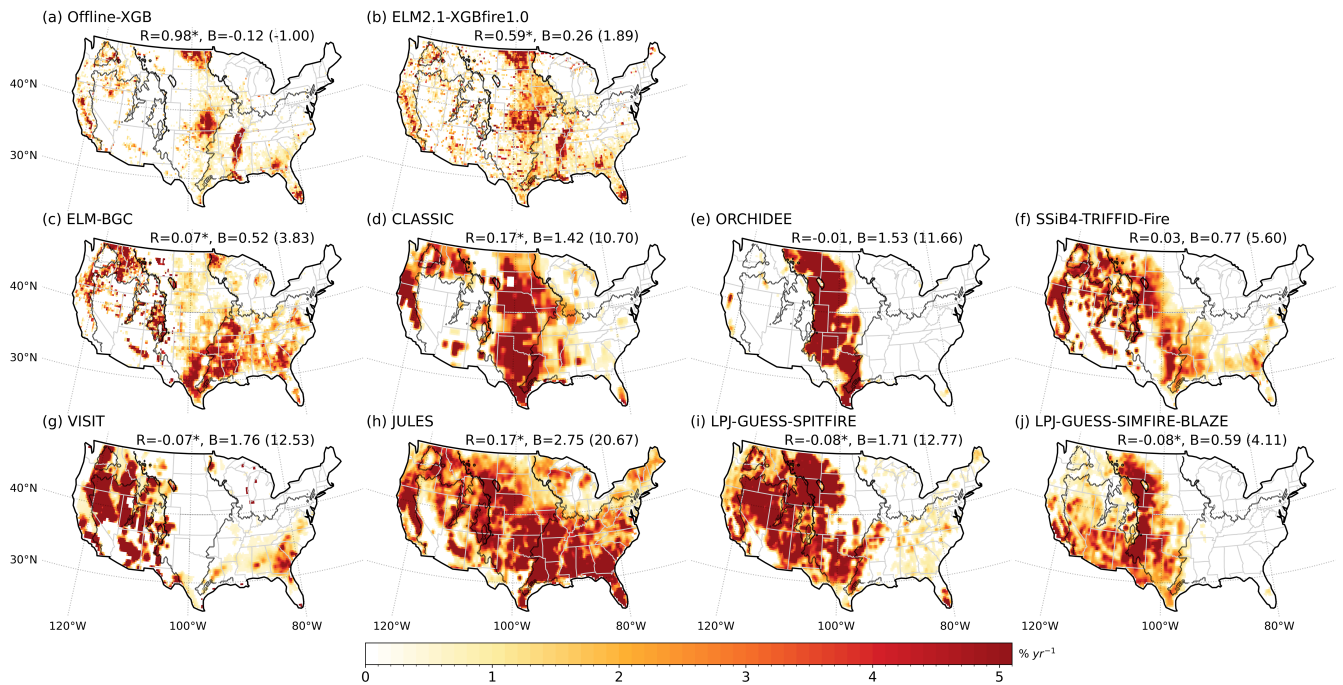


Figure 4: Same as Figure 3, but shows model outputs. The pattern correlation (R) and bias (B) against GFED5 are denoted.

In various ecoregions, the offline-XGB model demonstrates minimal biases, and the ELM2.1-XGBfire1.0 consistently outperforms all process-based fire models in predicting annual mean burned area (Fig. 4a-b). The accurate simulation of burned area over the Western Forest Mountains indicates that the ELM2.1-XGBfire1.0 framework generally captures the complex interplays between climate, vegetation, and human activities, with both climate forcings and predicted vegetation status from ELM-BGC. Meanwhile, the ELM2.1-XGBfire1.0 shows superior performance over the Great Plains, indicating that the ML model effectively describes crop fire thereby utilizing data on crop fraction and LAI.

The performance of the eight process-based fire models in simulating burned areas over the CONUS shows both strengths and weaknesses (Figs. 4c-j and Fig. 5). All models generally capture the high burned areas in key regions such as the WUS and Southeast U.S., except for ORCHIDEE showing a concentrated burned area in the Great Plains and LPJ-GUESS-SIMFIRE-BLAZE models missing fires in SE U.S. However, all process-based models tend to overestimate burned areas in various regions across the CONUS. ELM-BGC has moderate overestimations over the CONUS, with 3.83 Mha yr⁻¹. The burned areas are doubled in CLASSIC, ORCHIDEE, JULES and VISIT simulations, with values up to 20.7 Mha yr⁻¹ (Fig. 4a).

In the Western Forest Mountains, where fuel is abundant due to dense forest coverage, all process-based models except ORCHIDEE simulate 2 to 5 times of GFED5 burned area. This overestimation can be related to many factors including overestimation of fuel combustibility and underrepresentation of anthropogenic fire suppression (Balch et al., 2017). In contrast, wildfires in the NA Desert are primarily constrained by the fuel load. ELM-BGC and CLASSIC produce smaller overestimations, while SSiB4-TRIFFID-Fire, VISIT, JULES, and LPJ-GUESS models significantly overestimate the burned

area (4–16 times of GFED5), likely due to overestimations of fuel load, which might be attributed to insufficient water stress on vegetation growth in the arid region (Liu and Xue 2020; Z. Zhang et al. 2015). Although none of the process-based models accurately capture the spatial distribution of burned area over the Great Plains (Fig. 1), ELM-BGC, SSiB4-TRIFFID-Fire, and VISIT produce comparable burned areas to observations while CLASSIC and ORCHIDEE overpredict them (4–7 times of GFED5). The inaccurate description of the spatial pattern and large inter-model spread in the Great Plains may be caused by inaccurate treatments of cropland fires and pasture fires (Donovan et al. 2020). As noted by Teckentrup et al. (2019) and Burton et al. (2024), none of the process-based models has activated the explicit cropland fire model. While LPJ-GUESS-SIMFIRE-BLAZE incorporates harvesting in pastures, reducing biomass and influencing fire dynamics, all other process-based vegetation models do not distinguish pastures from natural grasslands for both vegetation growth and fire processes. Therefore, information on how fuel properties, including amount as well as physical (e.g., bulk density) and chemical characteristics, and fire ignitions differ between pastures and natural grasslands could help to improve burned area simulation in the process-based fire models (Rabin et al. 2017). Fuel management practices, such as prescribed burning and grazing, can significantly alter fire dynamics but are generally absent in current models. In the eastern U.S. (EUS) forests (Southeast and Northeast Temperate Forests ecoregions), fires are more managed by prescribed burning, leading to fewer uncontrolled extreme wildfires. Although prescribed burning as an additional ignition source is not included in the process-based models, ignition is not a limiting factor in this region due to the abundance of lightning, which provides sufficient natural ignition sources. Consequently, the burned area is primarily controlled by fire spread, which is influenced by natural conditions such as fuel availability and wind, allowing the models to perform well in simulating fire dynamics.

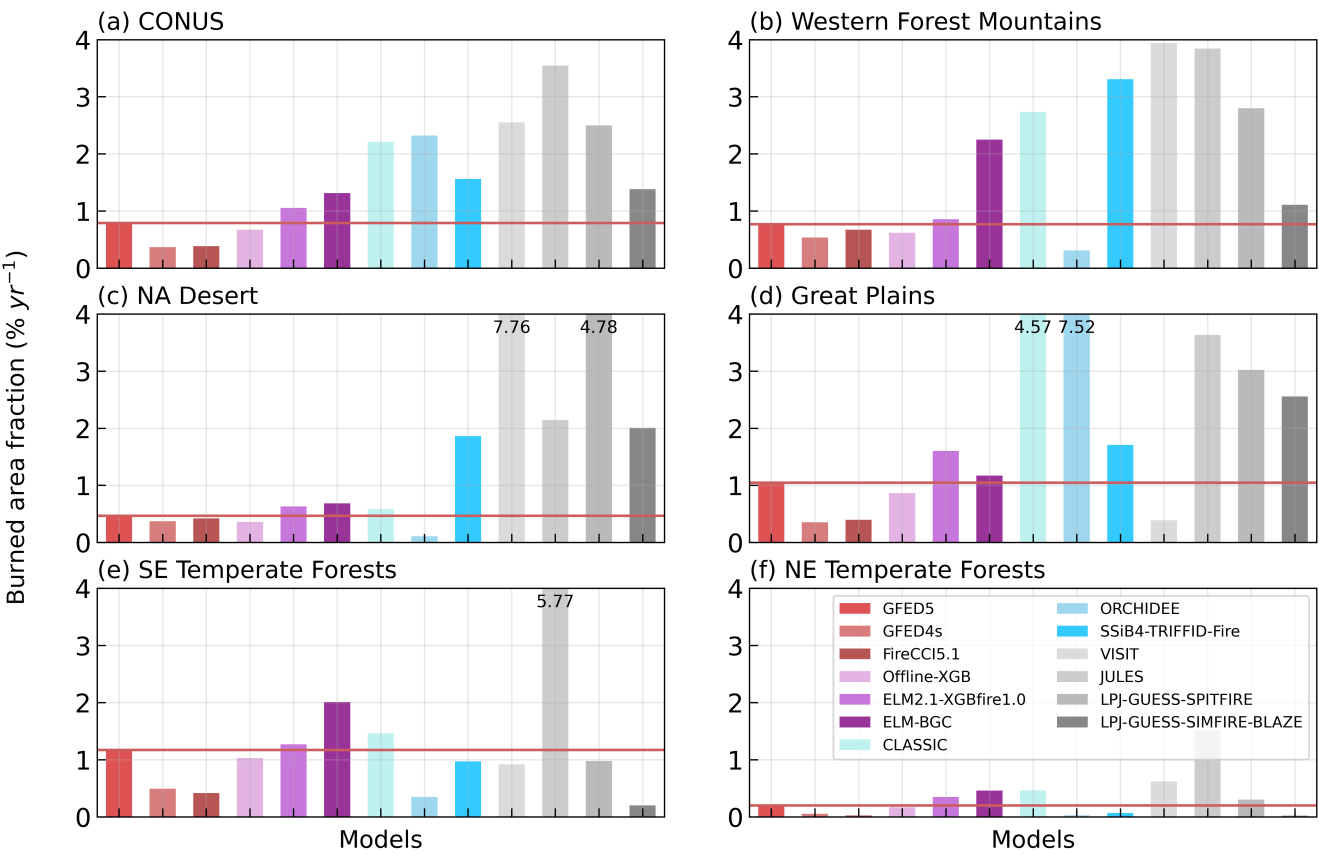
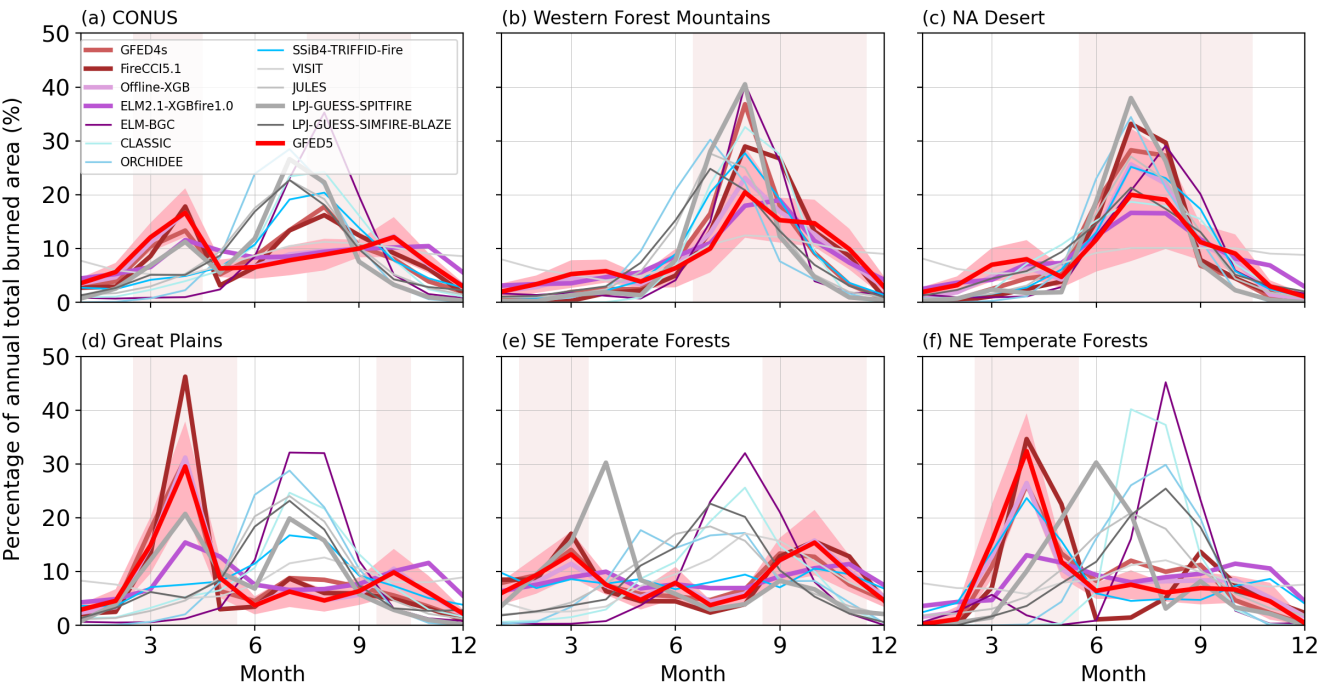


Figure 5: Observed and simulated mean burned area fraction (% yr⁻¹) over the CONUS and eco-regions. The red line in each panel indicates the observed burned area. Modeled burned areas greater than 4 % yr⁻¹ are truncated with the value denoted on the bar.

3.2 Evaluation of the burned area temporal variability

We evaluate the model performance in simulating the monthly burned area and depicting fire seasons. Fire season is defined as a monthly burned area greater than 1/12 of the annual total burned area. The CONUS has two fire seasons, i.e., March-April-May and August-September-October, affected by both climate and human activities (Fig. 6a). The WUS fire season spans from early summer to late fall, primarily determined by the dry conditions and high temperature during these months (Safford et al. 2022; Schoennagel et al. 2017). Specifically, over the Western Forest Mountains, the fire season includes July to November (Fig. 6b). Most models capture the July to October fire season, except for ORCHIDEE (May-August). However, only offline-XGB, SSiB4-TRIFFID-Fire, and CLASSIC simulate the peak fire month in August, while others simulate a peak ~1–2 months late. Similar fire season and model performance are observed over the NA Desert (Fig. 5c). In wildfire-dominant regions, the shift in fire peak months might be related to the representation of seasonality in vegetation production and fuel build-up in the BGC model (Hantson et al. 2020).

Human activities can also change the timing of fire occurrence (Le Page et al. 2010). Over the Great Plains, pasture fires are conducted during late winter to early spring to control pests, recycle nutrients, and prepare fields for planting (Gates et al. 2017). During the late summer to early fall, crop fires are conducted to clear crop residues. However, these fires may become uncontrolled, leading to larger fires that significantly impact the region. The fire seasons due to pasture fires and crop fires are evident in observations and are captured in offline-XGB and ELM2.1-XGBfire1.0, despite ELM2.1-XGBfire1.0 slightly underestimating the peak in March. Except for LPJ-GUESS-SPITFIRE, none of the process-based models is able to simulate these periods, instead, a summer fire season is predicted. LPJ-GUESS-SPITFIRE produces peaks in both spring and summer. In SE Temperate Forests, routinely prescribed burns reduce large fire occurrences across the year (Mitchell et al. 2014). The dry condition and/or fallen vegetation fuel larger burned areas in February–March and September–November. The ML-based models generally reproduce the fire seasons in March–April and September–November while none of the process-based models captures the bimodal seasonality. The results of NE Temperate Forests are similar to Great Plains, expect no peak burned area appears in November. The offline-XGB and SSiB4-TRIFFID-Fire capture the spring peak. To the best of our knowledge, ELM-BGC is one of the few process-based models capable of explicitly simulating crop fires; however, this feature was not enabled in our study. None of the models used here include explicit representations of pasture burning. Our evaluation suggests that including anthropogenic fires could help to improve model simulations in Central and Eastern US. However, this requires a better understanding of how fire is used for land management under different socioeconomic and cultural conditions (Pfeiffer et al., 2013; Li et al., 2013).



325

326

327

Figure 6: Monthly mean burned area fraction (% yr⁻¹) over each eco-region. Vertical shadings indicate the fire seasons, monthly burned area greater than 1/12 of the total burned area, shadings along x-axes indicate one-standard deviation across the years.

328

329

330

331

332

333

Over the CONUS, the observed interannual variability (IAV), measured using standard deviation, is 0.7 Mha yr⁻¹, representing 12% of the annual total burned area in GFED5 (Fig. 7a). GFED4s and FireCCI5.1 suggest 1.1 Mha yr⁻¹ (45%) and 0.9 Mha yr⁻¹ (30%), respectively. Process-based models greatly overestimate the IAV, ranging from 2.5 (LPJ-GUESS-SIMFIRE-BLAZE) to 6.6 (VISIT) Mha yr⁻¹. The relative IAV regarding the modeled annual mean value, ranging from 12% (JULES) to 41% (ELM-BGC), generally within the range of observations. The machine learning models, offline-XGB and ELM2.1-XGBfire1.0 produce IAV of 0.6 Mha yr⁻¹ (11%) and 0.8 Mha year⁻¹ (10%), respectively.

334

335

336

337

Despite the magnitude of IAV being amplified by process-based models, after extracting the mean values and dividing by standard deviation, the standardized time series well correlated with the observation (Fig. 7b). Since the modeled IAV is generally influenced by climate variability and the climate-driven fuel variability, both process-based and ML-based models capture the timing of the fluctuations.

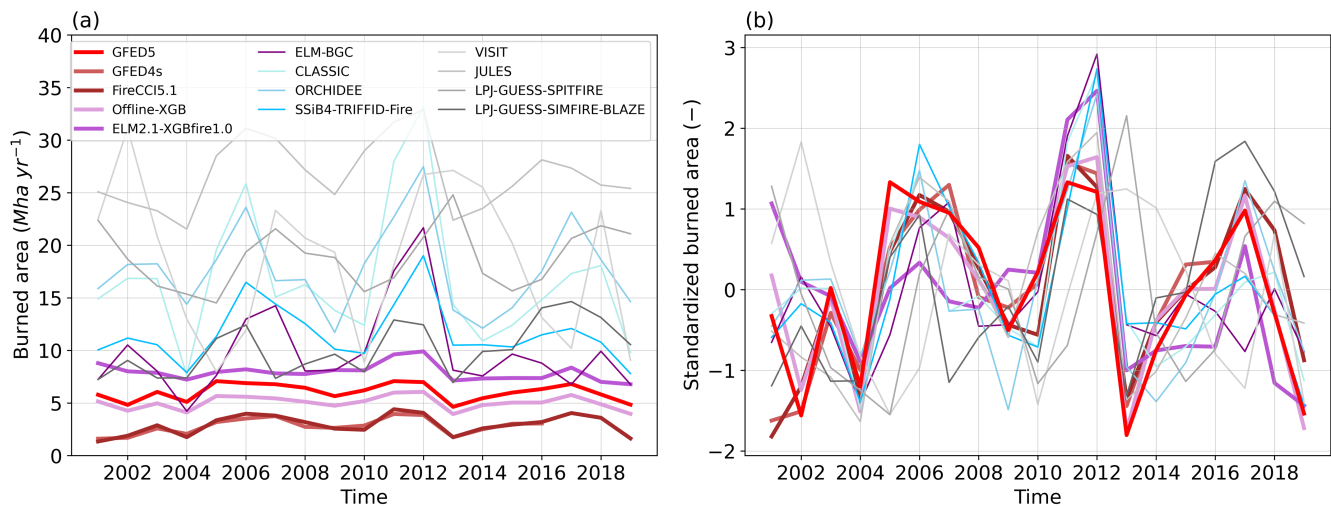


Figure 7: Annual total burned area (Mha yr⁻¹). (a) Annual total and (b) standardized by removing mean and standard deviation.

Monthly temporal variability in burned areas demonstrates significant regional differences across the eco-regions (Fig. 8). Over the entire simulation period, the ML-based models generally capture the timing of wildfires across the CONUS with a temporal correlation coefficient greater than 0.5 ($p < 0.01$), whereas the process-based models exhibit a correlation of only 0.3 ($p > 0.01$). The ML-based models also effectively capture the temporal variability across the eco-regions, although there is a slight decrease in the ELM2.1-XGBfire1.0 in the Great Plains and EUS. This decrease is likely related to the fire-vegetation feedback, which alters the fuel condition differently from the training set. In contrast, the process-based models show comparable correlations as the ML-based models in the WUS but fail to accurately predict burned area temporal variations in the Great Plains and EUS. Again, climatic factors play a dominant role in shaping the temporal variability of BAF in the WUS, while human activities largely influence the BAF in the Great Plains and EUS (Kupfer et al. 2020; Y. Chen et al. 2023). Process-based models tend to better describe responses of fuel load and combustibility to climate than responses of fire ignition and suppression to human activities (Hantson et al. 2016).

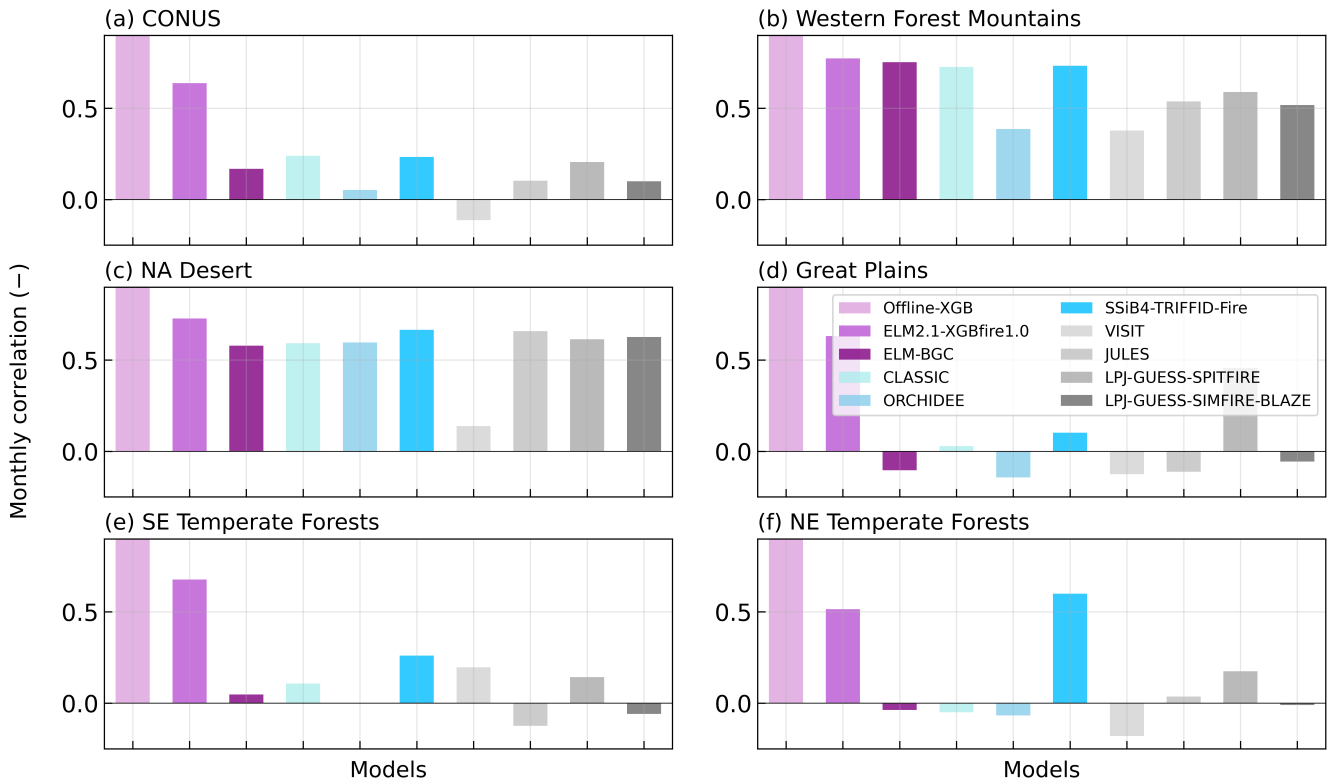


Figure 7: Monthly correlation coefficient between simulations and GFED5 over each eco-region.

4 Discussion and Conclusion

4.1 Overview of the hybrid framework

This study introduces a hybrid framework integrating an XGBoost wildfire model into an Earth system model (ELM-BGC), resulting in ELM2.1-XGBfire1.0. Both offline and coupled versions of the ML model were evaluated against observations and compared to eight state-of-the-art process-based models. The offline-XGB significantly reduces burned area biases, particularly in the WUS, while the ELM2.1-XGBfire1.0 retains the spatial and temporal accuracies with slightly reduced performances. In regions such as the Great Plains and EUS, where human activities are major influences, offline-XGB and ELM2.1-XGBfire1.0 outperform all process-based models.

4.2 Challenges and insights for process-based models

We acknowledge that the simulation biases in process-based models may come from multiple sources. All ISIMIP3a fire models were driven by daily GSWP3-W5E5 forcings at a 0.5° spatial resolution. Differences in forcing data could lead to variations in burned area predictions. However, given that both ELM-BGC and ELM2.1-XGBfire1.0 are driven by the same set of forcings yet produce markedly different burned area predictions, we suggest that limitations in physical understanding may play a dominant role in hindering the performance of the process-based model. By contrast, the ML model incorporates

the crop PFT fraction and is trained with data that include agricultural burning, allowing it to capture burning patterns often missing or underrepresented in process-based models. Meanwhile, all process-based fire models used in this study have used GFED4s or earlier versions as a reference for calibration. GFED5 captures significantly more small fires compared to GFED4s, making the CONUS annual burned area increase by 156%, with crop fire increasing by 240% (Chen et al., 2023). The inclusion of crop fires is particularly impactful in the CONUS.

The process-based fire models used in this study differ in both fire models and DGVMs. VISIT, JULES, LPJ-GUESS-SIMFIRE-BLAZE employs the semi-empirical fire models (Thonicke et al. 2001; Pechony and Shindell 2009; Knorr et al. 2014), in which burned area is calculated without an explicit rate-of-spread model (Hantson et al. 2016). The CLM-Li fire model (Li et al., 2012), a fire model of intermediate complexity, is incorporated into both ELM-BGC and SSiB4-TRIFFID-Fire and partially used in CLASSIC (Melton and Arora, 2016). Consequently, similar performance is observed among these models, although CLASSIC tends to exhibit larger overestimation. The highly complex SPITFIRE model (Thonicke et al. 2010) provides a more comprehensive description of fire behavior (e.g., fire duration and flame height) and is coupled with ORCHIDEE and LPJ-GUESS to describe the fire impact depending on plant traits (bark thickness and crown height). Although SPITFIRE provides more comprehensive description of fire, it does not outperform other fire models in regard to burned area simulation (Hantson et al. 2020).

With more sophisticated parametrization and fire parameters introduced, more observational analyses are required to understand the mechanism behind and to constrain the parametric uncertainty. The fire-vegetation feedbacks further complex this problem with more complex dynamic vegetation models are difficult to reach equilibrium after disturbances and the choice of prescribed or dynamic vegetation could also play a role (note that among all the process-based models, CLASSIC, VISIT, and ELM used prescribed vegetation while all others used dynamic vegetation. It is noteworthy that parameters involved in wildfire prediction are calibrated to align with the research interests of the institute developing and managing these models. Advancing the physical understanding wildfire processes for the CONUS and fine-tuning model parameters towards the new burned area dataset hold the potential to improve model performance (Huang et al., 2020).

4.3 Impact on carbon dynamics and broader application

Although ELM2.1-XGBfire1.0 significantly improves the simulation of burned areas, its impact on terrestrial carbon fluxes remains limited. Within the CONUS, fires primarily affect the terrestrial carbon cycle at localized scales due to the relatively small burned areas. ELM-BGC, for instance, underestimates gross primary production (GPP) by approximately 30% (figure not shown). With more accurate fire predictions, ELM2.1-XGBfire1.0 helps to slightly reduce this negative bias (less than 1%). Additionally, while ELM-BGC using prescribed PFT distributions can suppress the effects of fires on the ecosystem, it does not account for fire-induced shifts in vegetation species, where species with greater resistance or fire-adaptive traits may gradually dominate. Nonetheless, the coupling remains valuable, especially when the model is configured at higher resolutions. It is particularly important for evaluating fire-induced tree mortality, post-fire recovery, fire emissions, and their subsequent impacts on air quality, cloud formation, and surface meteorology, particularly when ELM is run as part of the E3SM.

400 The development and application of ML4Fire-XGB represent a significant step forward in our ability to model wildfire
401 dynamics in regions with complicated interactions between fires, ecosystems, climate, and human activities, bypassing the
402 explicit understanding of physical processes. By incorporating ML wildfire model into a land surface model, we address the
403 critical need for enhanced predictive capabilities at subseasonal to seasonal scales. Meanwhile, the predictability can adapt to
404 the evolving nature of fire regimes under climate change. This research not only contributes to the scientific community's
405 understanding of fire-ecosystem-climate interactions but also provides a practical tool for policymakers and resource managers
406 engaged in wildfire preparedness and response.

407 **Author contribution**

408 Research conceptualization, paper preparation, and analysis were performed by YL and HH. ELM configuration and set
409 up was supported by DX. The hybrid model coupling framework was first developed by TZ. The GFED5 data was provided
410 by YC. The ML fire model development was assisted by SSW. YL, HH, DX, TZ and YC contributed to the paper edits and
411 technical review.

412 **Acknowledgments**

413 This research has been supported by the Earth and Biological Sciences Directorate (EBSD)'s Laboratory Directed Research
414 and Development (LDRD) Program at Pacific Northwest National Laboratory (PNNL). D.X. was supported by the Earth
415 System Model Development program area of the U.S. Department of Energy, Office of Science, Office of Biological and
416 Environmental Research as part of the multiprogram, collaborative integrated Coastal Modeling (ICoM) project. PNNL is
417 operated by DOE by the Battelle Memorial Institute under contract DE-A05-76RL0 1830. Research activity at BNL was under
418 the Brookhaven National Laboratory contract DE-SC0012704.

419 **Conflict of Interest**

420 The authors declare that they have no conflict of interest.

421 **Data Availability**

422 Data and scripts used to generate results in this study are publicly available at PNNL's DataHub
423 (<https://doi.org/10.25584/2424127>). The Fortran-Python interface (ML4ESM) for developing ML parameterizations is
424 archived at <https://doi.org/10.5281/zenodo.11005103> (Zhang et al., 2024). The E3SM v2.1 (including ELM v2.1) is available
425 at <https://doi.org/10.11578/E3SM/dc.20230110.5> and <https://github.com/E3SM-Project/E3SM/releases/tag/v2.1.0> (E3SM

Project, 2023). The modified ELM v2.1 (including the XGBoost ML fire model) is available at <https://doi.org/10.5281/zenodo.13358187> (Liu et al., 2024).

Reference

- Andela, N., D. C. Morton, L. Giglio, Y. Chen, G. R. van der Werf, P. S. Kasibhatla, R. S. DeFries, et al. 2017. “A Human-Driven Decline in Global Burned Area.” *Science (New York, N.Y.)* 356 (6345): 1356–62.
- Arora, Vivek K., and George J. Boer. 2005. “A Parameterization of Leaf Phenology for the Terrestrial Ecosystem Component of Climate Models.” *Global Change Biology* 11 (1): 39–59.
- Balch, Jennifer K., Bethany A. Bradley, John T. Abatzoglou, R. Chelsea Nagy, Emily J. Fusco, and Adam L. Mahood. 2017. “Human-Started Wildfires Expand the Fire Niche across the United States.” *Proceedings of the National Academy of Sciences* 114 (11): 2946–51.
- Beguería, Santiago, Sergio M. Vicente-Serrano, Fergus Reig, and Borja Latorre. 2014. “Standardized Precipitation Evapotranspiration Index (SPEI) Revisited: Parameter Fitting, Evapotranspiration Models, Tools, Datasets and Drought Monitoring.” *International Journal of Climatology* 34 (10): 3001–23.
- Buch, Jatan, A. Park Williams, Caroline S. Juang, Winslow D. Hansen, and Pierre Gentine. 2023. “SMLFire1.0: A Stochastic Machine Learning (SML) Model for Wildfire Activity in the Western United States.” *Geoscientific Model Development* 16 (12): 3407–33.
- Burton, Chantelle, Richard Betts, Manoel Cardoso, Ted R. Feldpausch, Anna Harper, Chris D. Jones, Douglas I. Kelley, Eddy Robertson, and Andy Wiltshire. 2019. “Representation of Fire, Land-Use Change and Vegetation Dynamics in the Joint UK Land Environment Simulator Vn4.9 (JULES).” *Geoscientific Model Development* 12 (1): 179–93.
- Burton, Chantelle, Li Fang, Stijn Hantson, Matthew Forrest, Anna Bradley, Eleanor Burke, Jinfeng Chang, et al. 2024. “ISIMIP3a Simulation Data from the Fire Sector.” ISIMIP Repository. <https://doi.org/10.48364/ISIMIP.446106>.
- Burton, Chantelle, Seppe Lampe, Douglas I. Kelley, Wim Thiery, Stijn Hantson, Nikos Christidis, Lukas Gudmundsson, et al. 2024. “Global Burned Area Increasingly Explained by Climate Change.” *Nature Climate Change*, 1–7.
- Chen, Tianqi, and Carlos Guestrin. 2016. “XGBoost: A Scalable Tree Boosting System.” In *Proceedings of the 22nd ACM SIGKDD International Conference on Knowledge Discovery and Data Mining*, 785–94. KDD ’16. New York, NY, USA: Association for Computing Machinery.
- Chen, Yang, Joanne Hall, Dave van Wees, Niels Andela, Stijn Hantson, Louis Giglio, Guido R. van der Werf, Douglas C. Morton, and James T. Randerson. 2023. “Global Fire Emissions Database (GFED5) Burned Area.” Zenodo. <https://doi.org/10.5281/ZENODO.7668423>.
- Chuvieco, Emilio, M. Lucrecia Pettinari, Joshua Lizundia Loiola, Thomas Storm, and Marc Padilla Parellada. 2019. “ESA Fire Climate Change Initiative (Fire_cci): MODIS Fire_cci Burned Area Grid Product, Version 5.1.” Centre for Environmental Data Analysis (CEDA). <https://catalogue.ceda.ac.uk/uuid/3628cb2fdb443588155e15dee8e5352>.
- Claverie, Martin, Junchang Ju, Jeffrey G. Masek, Jennifer L. Dungan, Eric F. Vermote, Jean-Claude Roger, Sergii V. Skakun, and Christopher Justice. 2018. “The Harmonized Landsat and Sentinel-2 Surface Reflectance Data Set.” *Remote Sensing of Environment* 219 (December): 145–61.

461 Cucchi, Marco, Graham P. Weedon, Alessandro Amici, Nicolas Bellouin, Stefan Lange, Hannes Müller Schmied, Hans
 462 Hersbach, and Carlo Buontempo. 2020. “WFDE5: Bias-Adjusted ERA5 Reanalysis Data for Impact Studies.” *Earth System*
 463 *Science Data* 12 (3): 2097–2120.

464 Donovan, Victoria M., Carissa L. Wonkka, David A. Wedin, and Dirac Twidwell. 2020. “Land-Use Type as a Driver of Large
 465 Wildfire Occurrence in the U.S. Great Plains.” *Remote Sensing* 12 (11): 1869.

466 Forkel, Matthias, Niels Andela, Sandy P. Harrison, Gitta Lasslop, Margreet van Marle, Emilio Chuvieco, Wouter Dorigo, et
 467 al. 2019. “Emergent Relationships with Respect to Burned Area in Global Satellite Observations and Fire-Enabled Vegetation
 468 Models.” *Biogeosciences* 16 (1): 57–76.

469 Gates, Emily A., Lance T. Vermeire, Clayton B. Marlow, and Richard C. Waterman. 2017. “Fire and Season of Postfire
 470 Defoliation Effects on Biomass, Composition, and Cover in Mixed-Grass Prairie.” *Rangeland Ecology & Management* 70 (4):
 471 430–36.

472 Giglio, Louis, Luigi Boschetti, David P. Roy, Michael L. Humber, and Christopher O. Justice. 2018. “The Collection 6 MODIS
 473 Burned Area Mapping Algorithm and Product.” *Remote Sensing of the Environment* 217 (October): 72–85.

474 Giglio, Louis, Wilfrid Schroeder, and Christopher O. Justice. 2016. “The Collection 6 MODIS Active Fire Detection Algorithm
 475 and Fire Products.” *Remote Sensing of the Environment* 178 (June): 31–41.

476 Haas, Henrique, Nathan G. F. Reaver, Ritesh Karki, Latif Kalin, Puneet Srivastava, David A. Kaplan, and Carlos Gonzalez-
 477 Benecke. 2022. “Improving the Representation of Forests in Hydrological Models.” *The Science of the Total Environment* 812
 478 (March): 151425.

479 Hall, Joanne V., Tatiana V. Loboda, Louis Giglio, and Gregory W. McCarty. 2016. “A MODIS-Based Burned Area
 480 Assessment for Russian Croplands: Mapping Requirements and Challenges.” *Remote Sensing of Environment* 184 (October):
 481 506–21.

482 Hanan, Erin J., Jianning Ren, Christina L. Tague, Crystal A. Kolden, John T. Abatzoglou, Ryan R. Bart, Maureen C. Kennedy,
 483 Mingliang Liu, and Jennifer C. Adam. 2021. “How Climate Change and Fire Exclusion Drive Wildfire Regimes at Actionable
 484 Scales.” *Environmental Research Letters: ERL [Web Site]* 16 (2): 024051.

485 Hantson, Stijn, Almut Arneth, Sandy P. Harrison, Douglas I. Kelley, I. Colin Prentice, Sam S. Rabin, Sally Archibald, et al.
 486 2016. “The Status and Challenge of Global Fire Modelling.” *Biogeosciences* 13 (11): 3359–75.

487 Hantson, Stijn, Douglas I. Kelley, Almut Arneth, Sandy P. Harrison, Sally Archibald, Dominique Bachelet, Matthew Forrest,
 488 et al. 2020. “Quantitative Assessment of Fire and Vegetation Properties in Simulations with Fire-Enabled Vegetation Models
 489 from the Fire Model Intercomparison Project.” *Geoscientific Model Development* 13 (7): 3299–3318.

490 Huang, Huilin, Y. Qian, N. G. McDowell, D. Hao, L. Li, M. Shi, K. Rittger, G. Bisht, and X. Chen. 2024. “Elevated Forest
 491 Loss after Wildfires in Moist and Cool Forests in the Pacific Northwest.”

492 Huang, Huilin, Yongkang Xue, Fang Li, and Ye Liu. 2020. “Modeling Long-Term Fire Impact on Ecosystem Characteristics
 493 and Surface Energy Using a Process-Based Vegetation–Fire Model SSiB4/TRIFFID-Fire v1.0.” *Geoscientific Model*
 494 *Development* 13 (12): 6029–50.

495 Huang, Huilin, Yongkang Xue, Ye Liu, Fang Li, and Gregory S. Okin. 2021. “Modeling the Short-Term Fire Effects on
 496 Vegetation Dynamics and Surface Energy in Southern Africa Using the Improved SSiB4/TRIFFID-Fire Model.” *Geoscientific*
 497 *Model Development* 14 (12): 7639–57.

498 Ito, Akihiko. 2019. "Disequilibrium of Terrestrial Ecosystem CO₂ Budget Caused by Disturbance-Induced Emissions and
499 Non-CO₂ Carbon Export Flows: A Global Model Assessment." *Earth System Dynamics* 10 (4): 685–709.

500 JEC. 2023. "Climate-Exacerbated Wildfires Cost the U.S. between 394 to 893 Billion Each Year in Economic Costs and
501 Damages."

502 Jones, Abigail M., Jeffrey M. Kane, Eamon A. Engber, Caroline A. Martorano, and Jennifer Gibson. 2023. "Extreme Wildfire
503 Supersedes Long-Term Fuel Treatment Influences on Fuel and Vegetation in Chaparral Ecosystems of Northern California,
504 USA." *Fire Ecology* 19 (1): 1–19.

505 Jones, Matthew W., John T. Abatzoglou, Sander Veraverbeke, Niels Andela, Gitta Lasslop, Matthias Forkel, Adam J. P. Smith,
506 et al. 2022. "Global and Regional Trends and Drivers of Fire under Climate Change." *Reviews of Geophysics* 60 (3).
507 <https://doi.org/10.1029/2020rg000726>.

508 Klein Goldewijk, Kees, Arthur Beusen, Jonathan Doelman, and Elke Stehfest. 2017. "Anthropogenic Land Use Estimates for
509 the Holocene – HYDE 3.2." *Earth System Science Data* 9 (2): 927–53.

510 Knorr, W., T. Kaminski, A. Arneth, and U. Weber. 2014. "Impact of Human Population Density on Fire Frequency at the
511 Global Scale." *Biogeosciences* 11 (4): 1085–1102.

512 Kupfer, John A., Adam J. Terando, Peng Gao, Casey Teske, and J. Kevin Hiers. 2020. "Climate Change Projected to Reduce
513 Prescribed Burning Opportunities in the South-Eastern United States." *International Journal of Wildland Fire* 29 (9): 764–78.

514 Lange, Stefan, Christoph Menz, Stephanie Gleixner, Marco Cucchi, Graham P. Weedon, Alessandro Amici, Nicolas Bellouin,
515 et al. 2021. "WFDE5 over Land Merged with ERA5 over the Ocean (W5E5 v2.0)." ISIMIP Repository.
516 <https://doi.org/10.48364/ISIMIP.342217>.

517 Lasslop, Gitta, Kirsten Thonicke, and Silvia Kloster. 2014. "SPITFIRE within the MPI Earth System Model: Model
518 Development and Evaluation." *Journal of Advances in Modeling Earth Systems* 6 (3): 740–55.

519 Lawrence, David M., Keith W. Oleson, Mark G. Flanner, Peter E. Thornton, Sean C. Swenson, Peter J. Lawrence, Xubin Zeng,
520 et al. 2011. "Parameterization Improvements and Functional and Structural Advances in Version 4 of the Community Land
521 Model." *Journal of Advances in Modeling Earth Systems* 3 (3). <https://doi.org/10.1029/2011ms000045>.

522 Le Page, Yannick, Duarte Oom, João M. N. Silva, Per Jönsson, and José M. C. Pereira. 2010. "Seasonality of Vegetation
523 Fires as Modified by Human Action: Observing the Deviation from Eco - climatic Fire Regimes." *Global Ecology and
524 Biogeography: A Journal of Macroecology* 19 (4): 575 – 88.

525 Li, F., S. Levis, and D. S. Ward. 2013. "Quantifying the Role of Fire in the Earth System--Part 1: Improved Global Fire
526 Modeling in the Community Earth System Model (CESM1)." *Biogeosciences* 10 (4): 2293–2314.

527 Li, F., X. D. Zeng, and S. Levis. 2012. "A Process-Based Fire Parameterization of Intermediate Complexity in a Dynamic
528 Global Vegetation Model." *Biogeosciences* 9 (7): 2761–80.

529 Li, Fa, Qing Zhu, William J. Riley, Lei Zhao, Li Xu, Kunxiaojuan Yuan, Min Chen, et al. 2023. "AttentionFire_v1.0:
530 Interpretable Machine Learning Fire Model for Burned-Area Predictions over Tropics." *Geoscientific Model Development* 16
531 (3): 869–84.

532 Li, Fang, Benjamin Bond-Lamberty, and Samuel Levis. 2014. "Quantifying the Role of Fire in the Earth System--Part 2:
533 Impact on the Net Carbon Balance of Global Terrestrial Ecosystems for the 20th Century." *Biogeosciences* 11 (5): 1345–60.

534 Li, Fang, and David M. Lawrence. 2017. "Role of Fire in the Global Land Water Budget during the Twentieth Century Due
535 to Changing Ecosystems." *Journal of Climate*. <https://doi.org/10.1175/jcli-d-16-0460.1>.

536 Liu, Ye, and Yongkang Xue. 2020. "Expansion of the Sahara Desert and Shrinking of Frozen Land of the Arctic." *Scientific
537 Reports* 10 (1): 4109.

538 Lizundia-Loiola, Joshua, Gonzalo Otón, Rubén Ramo, and Emilio Chuvieco. 2020. "A Spatio-Temporal Active-Fire
539 Clustering Approach for Global Burned Area Mapping at 250 m from MODIS Data." *Remote Sensing of Environment* 236
540 (111493): 111493.

541 Mangeon, Stéphane, Apostolos Voulgarakis, Richard Gilham, Anna Harper, Stephen Sitch, and Gerd Folberth. 2016.
542 "INFERNO: A Fire and Emissions Scheme for the UK Met Office's Unified Model." *Geoscientific Model Development* 9 (8):
543 2685–2700.

544 Mathison, Camilla, Eleanor Burke, Andrew J. Hartley, Douglas I. Kelley, Chantelle Burton, Eddy Robertson, Nicola Gedney,
545 et al. 2023. "Description and Evaluation of the JULES-ES Set-up for ISIMIP2b." *Geoscientific Model Development* 16 (14):
546 4249–64.

547 Melton, Joe R., Vivek K. Arora, Eduard Wisernig-Cojoc, Christian Seiler, Matthew Fortier, Ed Chan, and Lina Teckentrup.
548 2020. "CLASSIC v1.0: The Open-Source Community Successor to the Canadian Land Surface Scheme (CLASS) and the
549 Canadian Terrestrial Ecosystem Model (CTEM) – Part 1: Model Framework and Site-Level Performance." *Geoscientific
550 Model Development* 13 (6): 2825–50.

551 Miller, J. D., H. D. Safford, M. Crimmins, and A. E. Thode. 2009. "Quantitative Evidence for Increasing Forest Fire Severity
552 in the Sierra Nevada and Southern Cascade Mountains, California and Nevada, USA." *Ecosystems* 12 (1): 16–32.

553 Mitchell, Robert J., Yongqiang Liu, Joseph J. O'Brien, Katherine J. Elliott, Gregory Starr, Chelcy Ford Miniati, and J. Kevin
554 Hiers. 2014. "Future Climate and Fire Interactions in the Southeastern Region of the United States." *Forest Ecology and
555 Management* 327 (September): 316–26.

556 Omernik, James M., and Glenn E. Griffith. 2014. "Ecoregions of the Conterminous United States: Evolution of a Hierarchical
557 Spatial Framework." *Environmental Management* 54 (6): 1249–66.

558 Parks, S. A., and J. T. Abatzoglou. 2020. "Warmer and Drier Fire Seasons Contribute to Increases in Area Burned at High
559 Severity in Western US Forests from 1985 to 2017." *Geophysical Research Letters* 47 (22).
560 <https://doi.org/10.1029/2020gl089858>.

561 Pechony, O., and D. T. Shindell. 2009. "Fire Parameterization on a Global Scale." *Journal of Geophysical Research:
562 Atmospheres* 114 (D16). <https://doi.org/10.1029/2009JD011927>.

563 Pfeiffer, Ruth M., Yikyung Park, Aimée R. Kreimer, James V. Lacey Jr, David Pee, Robert T. Greenlee, Sandra S. Buys, et
564 al. 2013. "Risk Prediction for Breast, Endometrial, and Ovarian Cancer in White Women Aged 50 y or Older: Derivation and
565 Validation from Population-Based Cohort Studies." *PLoS Medicine* 10 (7): e1001492.

566 Prentice, S. A., and D. Mackerras. 1977. "The Ratio of Cloud to Cloud-Ground Lightning Flashes in Thunderstorms." *Journal
567 of Applied Meteorology and Climatology* 16 (5): 545–50.

568 Rabin, Sam S., Joe R. Melton, Gitta Lasslop, Dominique Bachelet, Matthew Forrest, Stijn Hantson, Jed O. Kaplan, et al. 2017.
569 "The Fire Modeling Intercomparison Project (FireMIP), Phase 1: Experimental and Analytical Protocols with Detailed Model
570 Descriptions." *Geoscientific Model Development* 10 (3): 1175–97.

571 Rodrigues, Marcos, and Juan de la Riva. 2014. "An Insight into Machine-Learning Algorithms to Model Human-Caused
572 Wildfire Occurrence." *Environmental Modelling & Software* 57 (July): 192–201.

573 Rogers, Brendan M., Amber J. Soja, Michael L. Goulden, and James T. Randerson. 2015. "Influence of Tree Species on
574 Continental Differences in Boreal Fires and Climate Feedbacks." *Nature Geoscience* 8 (3): 228–34.

575 Rothermel, Richard C. 1972. *A Mathematical Model for Predicting Fire Spread in Wildland Fuels*. Intermountain Forest &
576 Range Experiment Station, Forest Service, U.S. Department of Agriculture.

577 Safford, Hugh D., Alison K. Paulson, Zachary L. Steel, Derek J. N. Young, Rebecca B. Wayman, and Morgan Varner. 2022.
578 "The 2020 California Fire Season: A Year like No Other, a Return to the Past or a Harbinger of the Future?" *Global Ecology*
579 *and Biogeography: A Journal of Macroecology* 31 (10): 2005–25.

580 Samborska, Veronika, Hannah Ritchie, and Max Roser. 2024. "Wildfires." *Our World in Data*.
581 <https://ourworldindata.org/wildfires>.

582 Schoennagel, Tania, Jennifer K. Balch, Hannah Brenkert-Smith, Philip E. Dennison, Brian J. Harvey, Meg A. Krawchuk,
583 Nathan Mietkiewicz, et al. 2017. "Adapt to More Wildfire in Western North American Forests as Climate Changes."
584 *Proceedings of the National Academy of Sciences* 114 (18): 4582–90.

585 Smith, Benjamin, I. Colin Prentice, and Martin T. Sykes. 2001. "Representation of Vegetation Dynamics in the Modelling of
586 Terrestrial Ecosystems: Comparing Two Contrasting Approaches within European Climate Space: *Vegetation Dynamics in*
587 *Ecosystem Models*." *Global Ecology and Biogeography: A Journal of Macroecology* 10 (6): 621–37.

588 Teckentrup, Lina, Sandy P. Harrison, Stijn Hantson, Angelika Heil, Joe R. Melton, Matthew Forrest, Fang Li, et al. 2019.
589 "Response of Simulated Burned Area to Historical Changes in Environmental and Anthropogenic Factors: A Comparison of
590 Seven Fire Models." *Biogeosciences* 16 (19): 3883–3910.

591 Thonicke, K., A. Spessa, I. C. Prentice, S. P. Harrison, L. Dong, and C. Carmona-Moreno. 2010. "The Influence of Vegetation,
592 Fire Spread and Fire Behaviour on Biomass Burning and Trace Gas Emissions: Results from a Process-Based Model."
593 *Biogeosciences* 7 (6): 1991–2011.

594 Thonicke, Kirsten, Sergey Venevsky, Stephen Sitch, and Wolfgang Cramer. 2001. "The Role of Fire Disturbance for Global
595 Vegetation Dynamics: Coupling Fire into a Dynamic Global Vegetation Model." *Global Ecology and Biogeography: A*
596 *Journal of Macroecology* 10 (6): 661–77.

597 Turco, Marco, John T. Abatzoglou, Sixto Herrera, Yizhou Zhuang, Sonia Jerez, Donald D. Lucas, Amir AghaKouchak, and
598 Ivana Cvijanovic. 2023. "Anthropogenic Climate Change Impacts Exacerbate Summer Forest Fires in California."
599 *Proceedings of the National Academy of Sciences of the United States of America* 120 (25): e2213815120.

600 Venevsky, Sergey, Kirsten Thonicke, Stephen Sitch, and Wolfgang Cramer. 2002. "Simulating Fire Regimes in Human -
601 dominated Ecosystems: Iberian Peninsula Case Study." *Global Change Biology* 8 (10): 984 – 98.

602 Villarreal, Miguel L., Laura M. Norman, Erika H. Yao, and Caroline R. Conrad. 2022. "Wildfire Probability Models Calibrated
603 Using Past Human and Lightning Ignition Patterns Can Inform Mitigation of Post-Fire Hydrologic Hazards." *Geomatics,*
604 *Natural Hazards and Risk* 13 (1): 568–90.

605 Wang, Sally S. - C, Yun Qian, L. Ruby Leung, and Yang Zhang. 2021. "Identifying Key Drivers of Wildfires in the
606 Contiguous US Using Machine Learning and Game Theory Interpretation." *Earth's Future* 9 (6): e2020EF001910.

607 Werf, Guido R. van der, James T. Randerson, Louis Giglio, Thijs T. van Leeuwen, Yang Chen, Brendan M. Rogers, Mingquan
608 Mu, et al. 2017. “Global Fire Emissions Estimates during 1997–2016.” *Earth System Science Data* 9 (2): 697–720.

609 Yue, C., P. Ciais, P. Cadule, K. Thonicke, S. Archibald, B. Poulter, W. M. Hao, et al. 2014. “Modelling the Role of Fires in
610 the Terrestrial Carbon Balance by Incorporating SPITFIRE into the Global Vegetation Model ORCHIDEE – Part 1: Simulating
611 Historical Global Burned Area and Fire Regimes.” *Geoscientific Model Development* 7 (6): 2747–67.

612 Zhang, Tao, Cyril Julien Morcrette, Meng Zhang, Wuyin Lin, Shaocheng Xie, Ye Liu, Kwinten Van Weverberg, and Joana
613 Rodrigues. 2024. “A FORTRAN-Python Interface for Integrating Machine Learning Parameterization into Earth System
614 Models.” *Authorea Preprints*. <https://doi.org/10.22541/essoar.171322761.17960693/v1>.

615 Zhang, Zhengqiu, Yongkang Xue, Glen MacDonald, Peter M. Cox, and G. James Collatz. 2015. “Investigation of North
616 American Vegetation Variability under Recent Climate: A Study Using the SSiB4/TRIFFID Biophysical/Dynamic Vegetation
617 Model.” *Journal of Geophysical Research, D: Atmospheres* 120 (4): 1300–1321.

618 Zhu, Qing, Fa Li, William J. Riley, Li Xu, Lei Zhao, Kunxiaojuan Yuan, Huayi Wu, Jianya Gong, and James Randerson. 2022.
619 “Building a Machine Learning Surrogate Model for Wildfire Activities within a Global Earth System Model.” *Geoscientific
620 Model Development* 15 (5): 1899–1911.

621 Zhuang, Yizhou, Rong Fu, Benjamin D. Santer, Robert E. Dickinson, and Alex Hall. 2021. “Quantifying Contributions of
622 Natural Variability and Anthropogenic Forcings on Increased Fire Weather Risk over the Western United States.” *Proceedings
623 of the National Academy of Sciences* 118 (45): e2111875118.